Optical band gap and the Burstein–Moss effect in iodine doped PbTe using diffuse reflectance infrared Fourier transform spectroscopy

2013 New J. Phys. 15 075020

(http://iopscience.iop.org/1367-2630/15/7/075020)

New Journal of Physics
The open access journal for physics

Optical band gap and the Burstein–Moss effect in iodine doped PbTe using diffuse reflectance infrared Fourier transform spectroscopy

Zachary M Gibbs[1], **Aaron LaLonde**[2] **and G Jeffrey Snyder**[2,3]

[1] Division of Chemistry and Chemical Engineering, California Institute of Technology, 1200 E California Boulevard, Pasadena, CA 91125, USA
[2] Department of Materials Science, California Institute of Technology, 1200 E California Boulevard, Pasadena, CA 91125, USA
E-mail: jsnyder@caltech.edu

New Journal of Physics **15** (2013) 075020 (18pp)
Received 26 February 2013
Published 23 July 2013
Online at http://www.njp.org/
doi:10.1088/1367-2630/15/7/075020

Abstract. Optical absorption edge measurements are performed on I doped PbTe using diffuse reflectance infrared Fourier transform spectroscopy. The Burstein–Moss shift, an increase in the absorption edge (optical band gap) with increasing doping level, is explored. The optical gap increases on the order of 0.1 eV for doping levels ranging from 3×10^{18} to 2×10^{20} cm^{-3}, relevant doping levels for good thermoelectric materials. Chemical potential is estimated from transport measurements—specifically, Hall effect and Seebeck coefficient—using a single band Kane model. In heavily doped semiconductors, it is well-known that the band gap shrinks with increasing doping level. This effect, known as band gap renormalization, is fit here using an $n^{1/3}$ scaling law which reflects an electron–electron exchange interaction. The renormalization effect in these samples is shown to be more than 0.1 eV, on the same order of magnitude as the band gap itself. Existing models do not explain such large relative changes in band gap and are not entirely self-consistent. An improved theory for the renormalization in narrow gap semiconductors is required.

[3] Author to whom any correspondence should be addressed.

Contents

1. Introduction 2
2. Experimental and theoretical methods 5
3. Results 6
4. Conclusions 14
Acknowledgments 15
References 15

1. Introduction

The maximum efficiency obtainable by a thermoelectric device is related to the dimensionless figure of merit, $zT = \frac{S^2\sigma}{\kappa}T$, where S is the thermopower (or Seebeck coefficient), σ is the electrical conductivity, κ is the thermal conductivity and T is the temperature. Each of the properties included in zT depends intimately upon the number of free carriers and electronic transport parameters of the material. These parameters arise from the materials' electronic band structure. Recent work on PbTe and other materials highlight the manipulation of these electronic states or 'band engineering' as a method for improving thermoelectric efficiency [1–4]. Band engineering in thermoelectric PbTe involves alloying and doping to modify the band structure in a way that improves the thermoelectric quality factor [4]. Of particular importance is the relative position of the primary and secondary transport bands that, as measured by the band gaps, can be modified with temperature, alloying and even doping.

PbTe alloys have some of the highest efficiencies for thermoelectric power generation, with zT values above 1 in the temperature range useful for waste heat recovery [1, 5–7]. In p-type PbTe a complex valence band structure exists that has been described with two valence bands: a lighter band at the L point (direct) and a heavier at the Σ line in the Brillouin zone [1, 2, 6, 8–17]. While the qualitative results of density functional theory (DFT) calculations show excellent agreement, band gap values and transport properties are known to be dependent on the specific approximations made such as the specific exchange/correlation functional, how the alloy is accounted for (e.g. supercell or Korringa–Kohn–Rostoker coherent potential approximation (KKR-CPA)), assumptions about the relaxation time and the effect of temperature.

Measurement of the optical properties directly investigates the electronic structure of the material giving a wealth of information useful for engineering thermoelectric properties [18]. Optical measurements can be used to estimate the energy difference between the valence and conduction bands, the band gap (E_g), which can help determine the electronic and thermoelectric properties of materials. At high temperatures, when $E_g \sim 3$ or $4k_BT$, the Fermi distribution is sufficiently broad such that a significant minority carrier population can develop, which results in a cancelling of a portion of the Seebeck voltage. Peltier heat currents from different carrier types exist even at zero net electrical current thereby leading to the bipolar thermal conductivity [19]. The presence of minority carriers in thermoelectric materials is the primary reason for reduction of zT at high temperatures.

There are several experimental methods of measuring the band gap, both using electronic and optical properties. First, the band gap can be estimated from electronic resistivity for an intrinsic semiconductor (where the number of holes and electrons are approximately equal), but this simple calculation assumes that both electrons and holes have the same mobility and that

it has a specific temperature dependence. Alternatively, the peak in the Seebeck coefficient that appears at high temperatures due to the influence of minority carriers can be used to estimate the band gap as $E_g = 2\alpha_{max}T$ [20], but again this requires similar assumptions about the relative mobility of holes and electrons. Because of the assumptions these methods can only give qualitative values (within 0.1 eV or ~30% in PbTe). For a more direct measurement of band gap, optical methods have been preferred.

Due to their ease of heavy doping and high electrical conductivity, thermoelectric materials are generally small band gap semiconductors with gaps in the mid infrared (0.1–0.5 eV). Optical measurements in PbTe were first performed in the 1950 and 1960s and showed a band gap of around 0.3 eV with a temperature dependence of $\frac{dE_g}{dT} = 0.3 \pm 0.1\,\text{meV K}^{-1}$ [21–24]. Prakash investigated the pressure dependence of the fundamental gap and determined that only about half of the change with temperature could be attributed to thermal expansion while the rest was probably due to interaction with phonons [25, 26]. Nikolic and others have studied the optical band gaps in a variety of lead chalcogenide alloys [27–30]. Several studies of p-type PbTe found evidence of a second valence band using optical methods through inter-valence band transitions below the fundamental absorption energy [9, 31]. Also, the formation of impurity states has been observed and their energies have been estimated using optical absorption for PbTe doped with In [32–34] and Tl [34, 35]. Other thin film and bulk absorption measurements of alloys and quantum wells are useful for design of infrared lasers and detectors [36–40]. While there are many optical measurements of the band gap, many studies do not consider the effects of free carriers on the fundamental absorption edge.

Many of the previous reports of optical band gap measurements on PbTe have used single crystal samples measured in transmission [22, 23, 25, 29–31, 41, 42]. Transmission experiments have a few disadvantages. Firstly, optically transparent single crystals are often used to avoid internal reflections and light scattering at the grain boundaries—which are generally more difficult to prepare than polycrystalline samples. Secondly, the samples must be polished extremely thin since the absorbance scales exponentially with the absorption coefficient and sample thickness through Beer's law. This limits the highest absorption coefficient that can be measured for a given sample thickness. Lastly, in cases where the samples were sufficiently thin (i.e. thin film samples with thicknesses on the order of the light wavelength), oscillations can result in the measured absorbance. These Fabry–Perot fringes are related to interference during internal reflection. While the effect can be mitigated through mathematical models, additional analysis is required.

Other methods of measuring the optical properties in lead chalcogenides have also been used. PbTe, being a narrow gap semiconductor, has been rather thoroughly studied for uses in infrared lasers and photodetectors. Other studies have measured specular reflectivity of PbTe samples which requires Kramers–Kronig analysis in order to obtain the absorption coefficient—inevitably, some extrapolation of the dielectric function is necessary which can complicate the analysis [43]. Spectroscopic ellipsometry can bypass the necessity for the Kramers–Kronig analysis by measuring both the real and imaginary components of the dielectric function simultaneously, and some studies of lead chalcogenides as photodetectors or infrared lasers use these techniques [37, 44]. Many of the optical measurements show the higher energy features (> 1 eV) of PbTe which can be important to determining critical points in the joint density of states—a convenient way to compare with DFT calculations [18, 45]. This work, however, will focus on the fundamental absorption edge.

Diffuse reflectance infrared Fourier transform spectroscopy (DRIFTS) was used exclusively in this work for optical measurements due to its ease of sample preparation and data analysis. Diffuse reflectance can be obtained in a thin sample layer of a ground powder. The measurement requires only a small amount of polycrystalline sample (100 mg or less). Because of the Fourier transform analysis, light at all frequencies can be measured simultaneously—greatly reducing sampling time. Relating the diffuse reflectance to sample absorption can be performed using the Kubelka–Munk function. This report shows that DRIFTS is very sensitive to small changes in the energy of direct transitions across the band gap due to progressively higher doping levels. With proper extrapolation the small shifts associated with doping can be shown and understood according to existing optical analysis techniques.

Heavily doped semiconductors, including most good thermoelectric materials, have free carrier contributions to the optical absorption that can complicate the estimate of the band gap. Often the band gap is simply assumed to be the extrapolation of the absorption edge to zero absorption. In the case of degenerately doped semiconductors, this can cause large errors in the estimate of the true band gap on the order of the value of the electrochemical potential, ζ, relative to the band edge (which can be more than 0.1 eV in heavily doped samples). Since the early 1950s, it has been known that for semiconductors with small effective mass, the band gap tends to change with increasing doping [46, 47]. These effects have been considered in lead chalcogenides by several authors [24, 48–50] using methods other than DRIFTS.

In the case of a degenerately doped n-type semiconductor, states near the conduction band edge have a nonzero occupancy. As a result, the photon energy required for excitation across a direct band gap becomes higher by an additional $(1 + \frac{m_c}{m_v})\zeta$ in the case of direct transitions (see figure 1) which results in an increase in the optical band gap, $E_{g,opt}$, known as the Burstein–Moss shift. The true band gap (E_g) remains unaffected with doping if we consider the rigid band approximation which assumes the band gap and band parameters are independent of the electron filling. This often used approximation has proven effective in electronic transport modeling for many thermoelectric materials over a wide range of temperatures and doping levels. The thermal gap, $E_{g,thermal}$, is relevant to transport properties and minority carrier excitation. The true band gap, E_g, has been shown both experimentally through optical measurements [51–53] and theoretically [51–53] to be reduced as the carrier concentration increases in heavily doped semiconductors—known as band gap renormalization. Renormalization is thought to be related to Coulombic repulsion of the electrons and/or exchange interactions.

The difference between the optical and true band gaps have been studied in many III–V and other semiconductors and semiconductor devices. It is important to have an understanding of band gap renormalization for a variety of semiconductor devices where both the majority and minority carrier concentration and specific band positions can be necessary to optimize performance. In thermoelectric materials, though, the effects of heavy doping on the optical properties are generally not considered. In fact, there is often no distinction made between the thermal and optical gaps in doped materials [54, 55]. While the differences can be circumvented in the case of an undoped material (PbTe undoped binary), some thermoelectric materials may include both shifts in the doping level and to the band structure itself. In this work, we attempt to quantify the Burstein–Moss shift on the optical gap, and gap renormalization in iodine doped PbTe using diffuse reflectance spectroscopy. We primarily use measured Seebeck coefficients to estimate the chemical potential which is an improvement to simply measuring the Hall carrier concentration. Further, we attempt to improve upon renormalization estimates by self-consistently considering the band gap parameter.

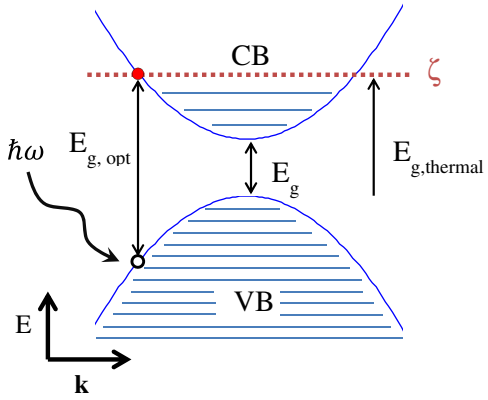

Figure 1. Optical band gap as a result of the Burstein–Moss shift in degenerately doped semiconductors.

2. Experimental and theoretical methods

PbTe samples were synthesized by melting and annealing. The ingots were hand-ground into a fine powder and hot pressed into 1/2 inch diameter discs using an induction hot press method described previously [56]. The particulars of their synthesis and electronic properties measurements are shown in a previous work [57].

Electronic properties measurements were used in conjunction with Boltzmann transport equation models and a single Kane type band which is outlined in detail by several references [1, 10, 58]. These models were used in order to obtain an estimate of the electrochemical potential ζ, which reduces to the chemical potential (ξ) in the absence of an applied electric field, for each sample; this was accomplished in two ways. Firstly, using room temperature Seebeck coefficient measurements, the electrochemical potential could be estimated assuming a single Kane band model where acoustic phonon scattering is assumed as the primary electron scattering mechanism. The single Kane band model has been shown to be a good model for the conduction bands in PbTe [57]. The band gap parameter in the Kane model was assumed to have a constant value near that of the undoped PbTe, 0.295 eV, for this analysis. Secondly, the electrochemical potential could be estimated for a given carrier concentration using a constant effective mass; the effective mass was obtained from fitting the room temperature Seebeck relation with Hall carrier concentration (Pisarenko plot), $m^*_{d0} = 0.276\, m_e$ was a reasonable value for these PbTe samples. Alternatively, the chemical potential could be estimated from Seebeck coefficient measurements directly without assumptions about the effective mass. While a six-band model could be used to improve chemical potential estimates at high doping ($>5 \times 10^{19}\,\mathrm{cm}^{-3}$) [16], the Kane model shows good agreement with transport properties and was used instead.

Samples were measured in diffuse reflectance with a Praying Mantis attachment using a Nicolet 6700 Fourier transform infrared spectrophotometer with a deuterated triglycine sulfate (DTGS) detector and KBr beamsplitter. All samples were referenced to the provided alignment mirror, this was found to give nearly same results as when referenced to KBr powder without the added impurity features from KBr itself. The absorption coefficient was obtained using Kubelka Munk analysis $F(R) = \frac{\alpha}{K} = \frac{(1-R)^2}{2R}$, where R is the fractional reflectance, α is the

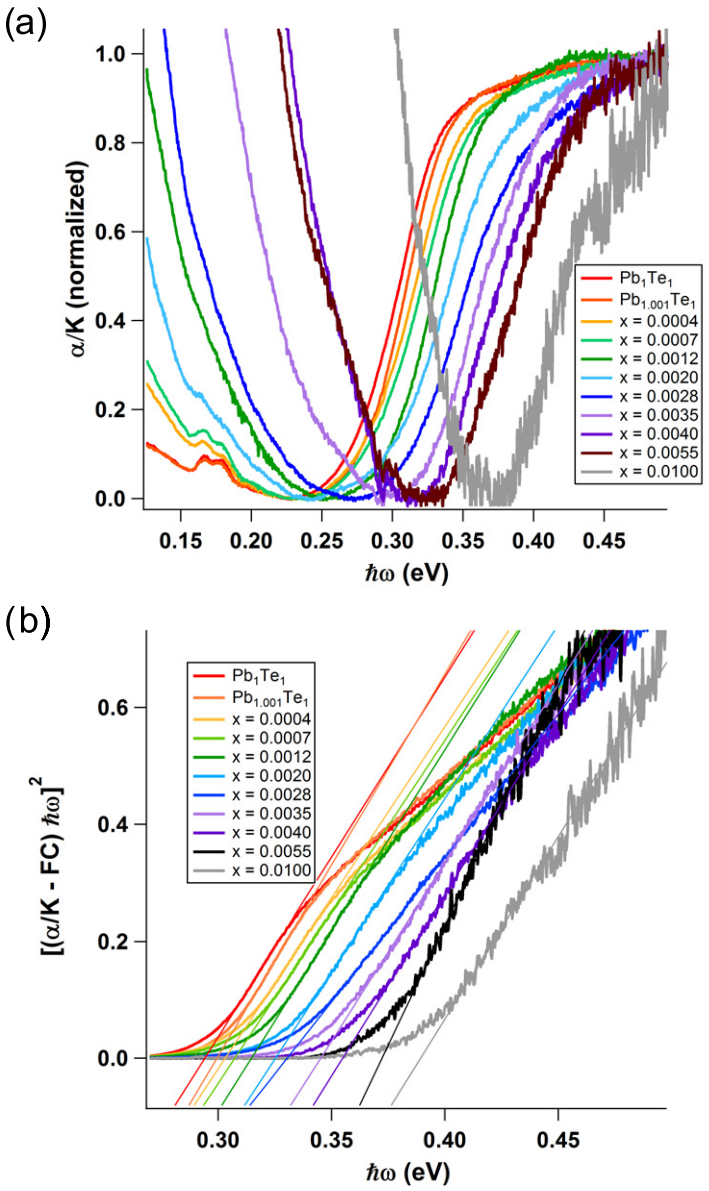

Figure 2. Normalized Kubelka Munk function for $PbTe_{1-x}I_x$ for (a) raw data, and (b) absorption coefficient direct gap fit along with the linear extrapolation to obtain the optical band gap from the Tauc method.

absorption coefficient and K is the scattering coefficient. For particle sizes greater than the light wavelengths measured (20–2 μm), the scattering coefficient is understood to be approximately independent of frequency [59].

3. Results

Each sample revealed an absorption edge near 0.3 eV (shown in figure 2(a)), but heavily doped samples also showed increasing absorption at low energy. For samples with high

doping ($>2\times10^{19}\,\mathrm{cm}^{-3}$), there was an observable peak in absorption. This corresponds to the downward peak in reflection associated with the oscillating electron plasma in the material near the plasma frequency, $\omega_\mathrm{p}=\sqrt{\frac{Ne^2}{\epsilon_\infty m_\mathrm{I}^*}}$ [60], where N is the electron concentration, e is the fundamental electronic charge, ϵ_∞ is screened dielectric constant and m_I^* is the inertial effective mass. For metals, the plasma frequency is in the ultraviolet and visible, but in heavily doped semiconductors it can exist into the far infrared. The location of the reflectivity minimum can also be used as an estimate for the optical effective mass of the charge carriers, but this was neither the focus of this work nor will it be explored in detail here. In order to isolate interband transitions, these features were fit and subtracted with a power law ($y=ax^b+c$). In almost all cases, the exponent, b, followed the expectation for Drude carriers of $b=-2$, but some deviations occurred for heavily doped samples which showed more clearly the plasma reflection minimum. This method was also compared to just normalizing the data to its minimum value, the resulting extrapolated band gap was consistently $\sim$5 meV lower for the fits with the free carrier contribution subtracted.

While the accepted view of PbTe is as a direct gap semiconductor, with evidence shown both experimentally [50, 61–63] and theoretically [14, 15, 64], some confusion as to whether PbTe was a direct or indirect gap semiconductor existed in early optical measurements of PbTe where some authors obtained good fits to $\alpha^{1/2}$ versus $\hbar\omega$ expected for indirect transitions [23, 41]. Similar to these reports, the absorption spectra in this work have a linear $\alpha^{1/2}$ versus $\hbar\omega$ region where the extrapolated band-gap energy is slightly lower ($\sim$30–60 meV) than those fit for direct transitions. Scanlon suggests that this difference can be attributed to indirect transitions where a phonon is absorbed [10, 23], although single phonon energies are at most 12 meV or less based on a Debye temperature of 140 K [65] and neutron scattering experiments [66]. Prakash suggests Scanlon's observation could also be interpreted as merely a coincidental fit due to the Urbach tail (exponential decrease in density of states below the band edge) [25]. Although, we believe that Prakash's interpretation is correct in PbTe, many materials do exhibit both indirect and direct transitions with some energy separation. For example, in germanium, both direct and indirect transitions exist with the indirect gap occurring first at about 0.63 eV and direct transitions beginning at 0.81 eV [67]. The indirect portion involves a slow rise in absorption coefficient over a long energy range ($\sim$100 cm^{-1} over $\sim$0.2 eV) while the direct absorption on the other hand gives a much steeper rise over a shorter period ($\sim10^4\,\mathrm{cm}^{-1}$ over $\sim$0.05 eV). As a result, the direct gap is much more easily observed particularly if both direct and indirect transitions occur at close to the same energies. The absorption coefficient of PbTe changes $\sim10^4\,\mathrm{cm}^{-1}$ over $\sim$0.05 eV [49, 68], suggesting it is a direct gap semiconductor. Recently, it has been suggested that the true gap value is convoluted by mid-gap defect states [18]. While these states may affect the measured optical band gap, we see no significant contribution from localized states in the transport properties which are characteristic of itinerant (delocalized) carriers giving metal-like transport behavior. Therefore, the measured absorption edge was assumed to be associated with the band edge in PbTe and not mid gap defect states, although defect states near the band edge could certainly play a role in band gap renormalization.

A series of PbTe samples doped with iodine (n-type) were measured using DRIFT spectroscopy, the normalized spectra are shown in figure 2(a). Free carrier absorption which scales as $(\hbar\omega)^{-2}$ in the classical limit is observed at low frequencies. As the doping level increases, the free carrier contribution to the absorption coefficient moves to higher and higher frequencies as expected from the Drude model, when $\omega\gg\tau^{-1}$: $\alpha_\mathrm{FC}\propto\frac{ne^2}{n_\mathrm{r}cm^*\tau\omega^2}$ where n is the

number of free carriers, e is the elementary charge of an electron, n_r is the real refractive index, c is the speed of light, τ is the Drude scattering time and ω is the photon frequency [69]. The free carrier absorption was subtracted for the analysis of the optical gaps. Optical band gaps were obtained using the Tauc method, where $(\alpha\hbar\omega)^2$ is extrapolated on a plot versus photon energy, $\hbar\omega$, to zero absorption (figure 2(b)) [60] which is based on direct transitions between parabolic bands. Other authors have plotted α^2 versus $\hbar\omega$ for fitting the direct gap [23], but regardless of the method the result is similar (within the measurement error: ~0.005 eV).

In heavily doped samples an optical band gap can be extracted in the same way, although it is not immediately clear the absorption should still have such a simple functional form. Several spectral features are observed near the absorption edge. First, many observers note an exponential increase in absorption just below the gap, known as an Urbach tail. The Urbach tail is thought to be related to the random distribution of impurity atoms in the material; we also observe an approximately exponential increase in absorption just below the band edge [60, 70]. Next, as electrochemical potential moves deeper into the band with doping level, there is a decrease in the number of available states near the band edge for an electron to be excited into. This effect, known as the Burstein–Moss shift [46, 48, 60, 71], means that a higher energy photon is required to produce the same amount of absorption—moving the absorption edge to higher energies. Lastly, the true band-gap E_g has been shown to decrease with heavy doping, known as band gap renormalization [51, 72–74]. The Burstein–Moss shift and renormalization effects will be discussed further below. In order to relate the measured optical band gap to the thermal gap, a chemical potential estimate is required.

In many cases, the chemical potential is estimated by the 0 K limit of the parabolic band as an estimate of the Fermi energy: 0 K limit as $E_f = \frac{\hbar^2}{2m^*}(3\pi^2 n)^{2/3}$ where m^* is the band effective mass [75–77]. While this may be a good estimate for degenerate systems (at low temperature, high doping) for materials with parabolic band shapes, a better estimate involves solving the more general temperature dependent expression $n = \int_0^\infty D(E) f(E, \zeta, T)\, dE$ where D is the density of states and f is the Fermi distribution function which is a function of the electron energy E, chemical potential ζ and temperature T. It is well known that many semiconductors, including lead chalcogenides, deviate significantly from parabolic behavior. Ravich has developed an adaptation of the Kane band model for application to the lead chalcogenides which has shown excellent agreement to experimental transport data [1, 10, 57]. Using Ravich's solution of the Kane band model applied to lead chalcogenides, n can be calculated by numerically integrating equation (1)

$$n = \int_0^\infty \frac{\sqrt{2} m_{d0}^* (k_B T)^{1/2} (\varepsilon + \varepsilon^2\beta)(1 + 2\varepsilon\beta)}{\pi^2 \hbar^3} (1 + \exp(\varepsilon - \eta))^{-1}\, d\varepsilon, \tag{1}$$

where m_{d0}^* is the band edge density of states effective mass, ε is the dimensionless energy $(= \frac{E}{k_B T})$, β is the non-parabolicity parameter $(= \frac{k_B T}{E_g}$ from Ravich) and η is the reduced electrochemical potential $(= \frac{\zeta}{k_B T})$. Calculation of the electrochemical potential as a function of the true carrier concentration is rather straightforward, but in order to compare to the Hall carrier concentration the Hall factor, r_H, is needed. Equations for the Hall factor and other relevant model parameters were obtained assuming acoustic phonon scattering in a single band as described in detail by Ravich *et al* [10] and Wang *et al* [58] and relevant parameters for PbTe were used following LaLonde *et al* [1] and Pei *et al* [57].

Using the Boltzmann transport equation, it is possible to obtain an estimate for the electrochemical potential, ζ, directly from the measured Seebeck coefficient with no assumption

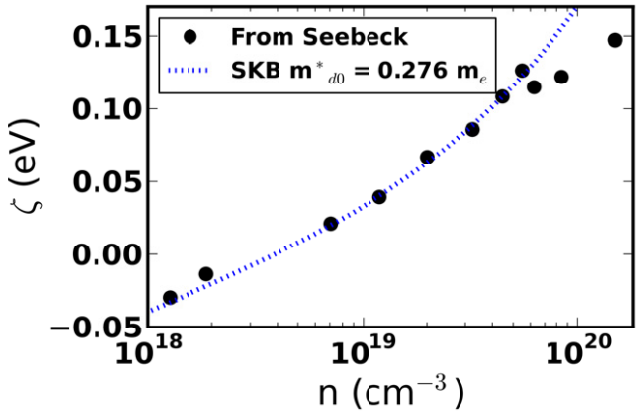

Figure 3. The change in electrochemical potential (calculated from the Seebeck coefficient) with Hall carrier concentration as a result of doping.

about the band edge effective mass (equation (2)) [10, 58]

$$S = \frac{k_B}{e}\left(\frac{{}^1F^1_{-2}}{{}^0F^1_{-2}} - \eta\right), \tag{2}$$

where ${}^nF^m_l = \int_0^\infty \left(-\frac{df}{d\varepsilon}\right)\varepsilon^n(\varepsilon+\beta\varepsilon^2)^m[(1+2\beta\varepsilon)+2]^{l/2}\,d\varepsilon$, a modified version of the Fermi integrals from Wang *et al* (figure 3) shows the calculated chemical potential for each iodine doped sample calculated using a single Kane band model both from the room temperature Seebeck measurements and using a constant band edge effective mass, $m^*_{d0} = 0.276m_0$ (best fit of the Seebeck versus n_H Pisarenko plot). Here, we can see the chemical potential for the most heavily doped samples increases to ∼0.15 eV from the band edge. It is important to note that the chemical potential estimate can vary depending on the particular band model. In the case of a single parabolic band, the chemical potential change to be as much as 50% higher for the same doping level. Once the electrochemical potential is known, it is possible to estimate the true gap from the optical gap measurement (figure 5(a)). As an alternative to the Tauc method, the gap can also be fit using the spectral Fermi distribution.

The Fermi distribution can be projected onto the unperturbed interband absorption as a multiplicative factor shown in equation (3). This technique and similar methods have been performed on a variety of materials, including lead chalcogenides [48, 49] and other materials [46, 51, 78, 79]:

$$\alpha(\hbar\omega) \propto \alpha_0(\hbar\omega)\,[1 - f(\hbar\omega, \zeta, T)], \tag{3}$$

α_0 is the absorption for an unpopulated conduction band; at $T = 0$ K which for parabolic bands is proportional to $\alpha_0 = \frac{\sqrt{\hbar\omega - E_g}}{\hbar\omega} = \frac{\sqrt{\hbar\omega - [E_{g,opt} - (1+\frac{m^*_c}{m^*_v})\zeta]}}{\hbar\omega}$. f is the Fermi distribution, which is related to the photon energy as $f(\hbar\omega, \zeta, T) = [1 + \exp(\frac{\hbar\omega - E_{g,opt}}{(1+\frac{m^*_c}{m^*_v})k_BT})]^{-1}$. The second term of equation (3) represents the electronic excitation probability based on the electron population from Fermi distribution. The electronic occupation probability is equal to 1/2 at the chemical potential which can then be related to the photon energy, $\hbar\omega$, assuming direct transitions and a fully occupied valence band ($E_g \gg k_BT$).

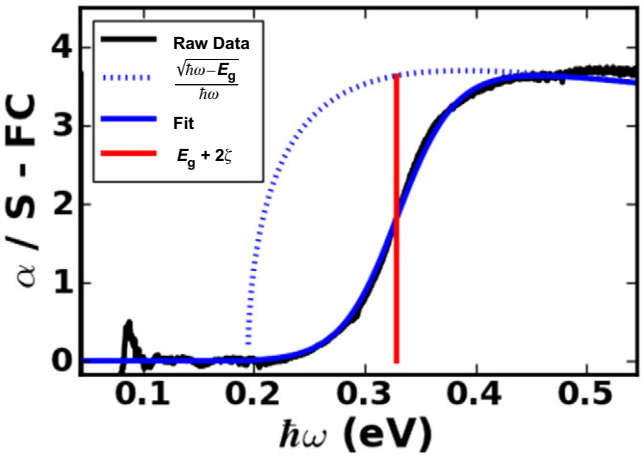

Figure 4. Fermi spectra method projecting the Fermi distribution onto the absorption edge in $PbTe_{1-y}I_y$, $y = 0.0012$ fit with a Fermi function.

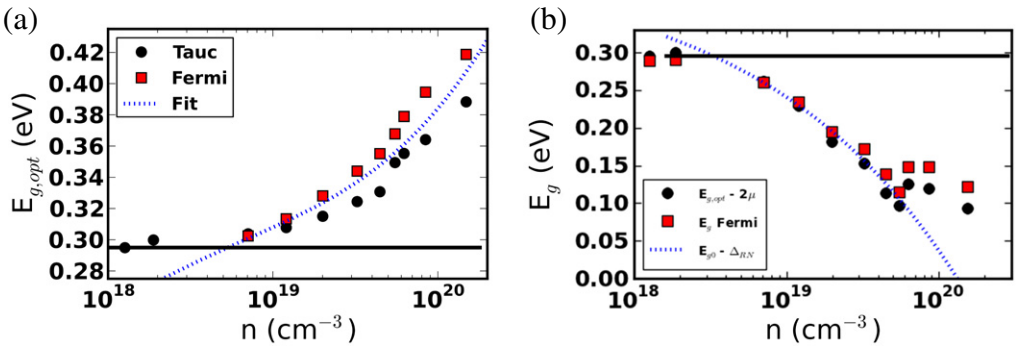

Figure 5. (a) Optical band gaps fit from optical data in two methods: extrapolation by the Tauc plot method and estimation from Fermi spectra fits. (b) The true band gap, calculated from the optical gaps by $E_g = E_{g,opt} - 2\zeta$. A fit is performed using all of the data and the renormalization as in equation (4).

Using a proportionality factor and the band gap value as a fitting parameter, it is possible to obtain an estimate for the optical band gap using equation (3) from the measured absorption spectra for a given estimate of the chemical potential (as estimated from either room temperature Seebeck and/or n_H measurements). The resulting fit is shown in figure 4. The optical and true gaps obtained by both the Tauc and Fermi spectra methods are shown in figures 5(a) and (b). Effectively, the Fermi projection method gives the optical band gap near the inflection point in the absorption (where the slope is the largest).

Two different methods have been used to calculate the band gap. The Tauc method takes the raw absorption data and extrapolates to estimate the optical gap while the Fermi spectra method projects the Fermi distribution onto the joint density of states which is fit to the measured absorption spectra to estimate the optical band gap. Figure 5(a) shows an increasing optical gap with doping level—a Burstein–Moss shift. As the doping level increases, the chemical potential in the conduction band moves upward which results in occupied states nearest the band edge which requires a higher energy photon for excitation of a carrier across the gap. The results

Table 1. Band gap and transport measurement results and chemical potential estimates for this series of samples. All Kane band calculations assume a constant β parameter of ~0.087 corresponding to the undoped sample band gap of 0.295 eV.

x	n_H (10^{18} cm^{-3})	S (μV K^{-1})	ζ_{Seeb} (eV)	ζ_{SKB} ($m^* = 0.276$) (eV)	$E_{g,opt}$ (eV)	$\Delta_{RN,Seeb}$ (eV)
0.0000	–	−275.0	−0.030	−0.033	0.295	–
0.0000	–	−230.0	−0.014	−0.022	0.300	–
0.0004	5.87	−141.4	0.021	0.020	0.304	0.033
0.0007	1.03	−109.6	0.039	0.040	0.308	0.066
0.0012	1.76	−81.9	0.067	0.063	0.315	0.114
0.0020	2.94	−66.9	0.086	0.089	0.324	0.142
0.0028	41.1	−52.0	0.108	0.108	0.331	0.181
0.0035	51.4	−43.0	0.126	0.123	0.349	0.199
0.0040	58.7	−42.9	0.115	0.132	0.355	0.170
0.0055	80.8	−41.5	0.122	0.156	0.364	0.175
0.0100	147	−33.7	0.147	0.208	0.388	0.201

from both the Tauc and Fermi spectra methods appear to agree within ±0.015 eV, although the broadening fits generally show a larger optical band gap. From figure 1, we can relate the optical gap to the true gap E_g.

Figure 5(b) shows the calculated true band gap with respect to doping level. In the case of direct transitions and similar valence and conduction band effective masses, the true band gap is related to the optical gap and the chemical potential as $E_g = E_{g,opt} - 2\zeta$. The result shows a true gap that decreases significantly with doping level relative to the undoped sample. This is a result of the measured optical gap not increasing nearly as quickly as expected. Over the same doping range, the optical band gap is expected to increase by 2ζ, which is as much as 0.25 eV at the highest doping levels—see figure 3. The measured optical band gap only increases by about 40% of the electrochemical potential value or ~0.07 eV at higher doping levels as shown in figure 5/table 1. The relatively small change of the optical band gap can be explained by the renormalization effect which is an estimate of band gap shrinkage with doping. The optical band gap increases according to equation (4) as described the schematic in figure 1 [71, 75, 76]:

$$E_{g,opt} = E_{g0} - \Delta_{RN} + \left(1 + \frac{m_c^*}{m_v^*}\right)\zeta, \tag{4}$$

where E_{g0} is the band gap of the undoped material, Δ_{RN} is the band gap renormalization, m_c^* and m_v^* are the conduction and valence band effective masses respectively, and ζ is the electrochemical relative to the conduction band edge. This equation again assumes direct transitions which is the reason that a factor greater than 1 is multiplying the electrochemical potential. The true band gap in equation (4) can be represented by $E_g = E_{g0} - \Delta_{RN}$ which accounts for a shrinking band gap with increasing doping level as shown in figure 5(b).

Both experimental and theoretical work has been done to determine how the band gap should change due to renormalization with increasing electron concentration in many semiconductors including: Si [51, 53, 74, 79, 80], Ge [80, 81], GaAs [73, 76], InP [52], ZnO [82] and other materials. The effect has proven important in semiconductor device applications

where the material's band gap determines many device characteristics and careful engineering is required to optimize performance. Gap narrowing is thought to be due to combination of effects including electron–electron exchange interactions, electron–donor interactions and band tailing [73, 75, 80, 83]. Electron–electron exchange has been shown to scale as $n^{1/3}$ in a weakly interacting free electron gas [80, 82]; this model is often used empirically, although the specific form may vary with crystal and energy band structure. The effect can be thought of as Coulombic repulsion between electrons in the material which scales as $1/r$ where r is the mean distance between electrons. Experimentally, attempts have been made to empirically fit the theoretical models. Most use a combination of power laws whose prefactors can in theory be calculated, but are most often used as fitting parameters [75, 80, 83]. Drabkin *et al* [49], for example, suggest that for PbTe a shift on the order of 10 meV is reasonable for doping levels on the order of 1×10^{19} cm^{-3}. When using the method of Mahan [83], however, the predicted reduction was 1 meV or less due to the large static dielectric constant ($\epsilon(0) \approx 400$) for PbTe. Following [51, 79], we fit the experimental renormalization (for both Tauc and broadening methods) to an $n^{1/3}$ power law, including an additional constant term: $\Delta_{\mathrm{RN}} = An^{1/3} + \Delta_{\mathrm{RN},0}$. The resulting renormalized fits to the optical and true band gap are plotted in figures 5(a) and (b) and are also shown in table 1.

Figure 5(b) shows the true band gap, when considering renormalization, reduces rather significantly. For the three most heavily doped samples, the chemical potential, as estimated from Seebeck coefficient measurements, does not continue to increase at the same rate. As a result, the true gap approaches an approximately constant value of close to 0.15 eV. The $n^{1/3}$ model deviates significantly for carrier concentrations $>\sim 6 \times 10^{19}$ cm^{-3}, resulting in a gap that rapidly approaches zero above this value. While the magnitude of the gap reduction is consistent with previously published results for heavily doped n-type PbTe [49], Si [51, 53, 79], Ge [81] and III–V semiconductors [52, 73, 75, 76, 84], the apparent discrepancy at high doping is not easily explained using the simple $n^{1/3}$ empirical model.

In Ravich's adaption of the Kane band model for lead chalcogenides, the band gap is a necessary parameter as it determines the non-parabolicity parameter—$\beta = \frac{k_B T}{E_g}$. Because optical measurements have shown evidence that the band gap in PbTe decreases with doping as a result of band gap renormalization, it might be expected to affect the energy dependence of the band structure. The band edge effective mass in narrow gap semiconductors has been suggested to scale with the band gap itself [10, 69]. Ravich suggests that the energy dependent effective mass for a Kane type band should scale with energy as

$$m^* = \frac{m_0 E_g}{2p^2}\left(1 + \frac{2E}{E_g}\right), \tag{5}$$

where p is the kp matrix element coupling states between two bands: $\langle u_1 | p | u_2 \rangle$. The first term will scale proportional to the band gap, while the second will scale with E, the electron energy. More often, the prefactor in equation (5) is treated as a constant—m_0^*, the band edge effective mass—which can be fit from the Seebeck coefficient versus carrier concentration Pisarenko plot. Optical measurements of the band gap renormalization in this work suggest that the gap decreases with increasing carrier concentration. In order to probe the effect that this might have on the estimate of the chemical potential and on the transport properties, a self-consistent approach should be taken. For all of the previous calculations, the chemical potential has been estimated from Seebeck coefficient (equation (2)) assuming a constant Kane-band nonparabolicity parameter (β used in equations (1) and (2)) given by assuming a constant band

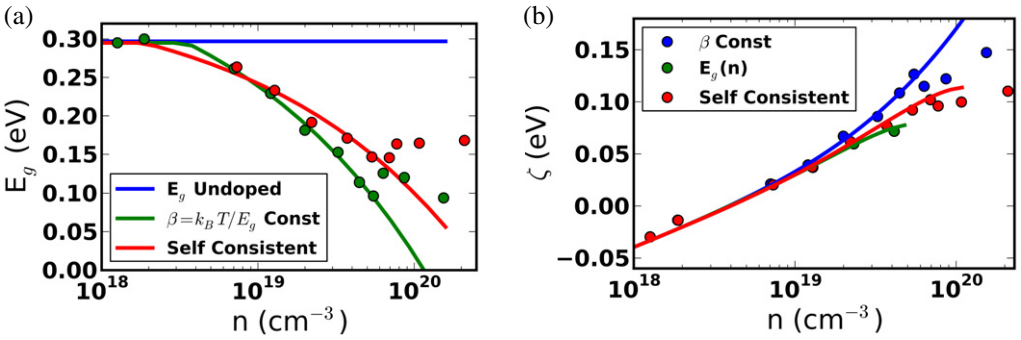

Figure 6. Iterative self-consistent calculation of the true gap $E_g(n)$ in accordance with the Kane band model. (a) The result of different n-dependences of the Kane β parameter solid points represent $E_g(n)$ in accordance with equation (4) (using the measured optical gaps and chemical potential estimates from Seebeck coefficient measurements). (b) The estimated chemical potential as a function of doping level for different dependence of β on n—lines represent constant effective band edge mass (equation (2), $m_0^* = 0.276\, m_0$) and points are calculated from Seebeck coefficient (equation (3)).

gap of 0.295 eV equal to that of the undoped PbTe sample. Using the fitted n-dependent gap: $E_g(n) = E_{g0} - \Delta_{RN}(n)$, we can self-consistently calculate n as a function of chemical potential with an n-dependent nonparabolicity parameter, $\beta = \frac{k_B T}{E_g(n)}$. The new value of chemical potential was used to recalculate the gap renormalization using the measured optical gaps—which was again fit to an $n^{1/3}$ model. After several iterations, the true gap appeared to converge to a self-consistent value that was slightly higher than the previous result which assumed constant gap. The self-consistent solution yielded renormalization fitting parameters of 5.6×10^{-8} eV cm and -0.068 eV for A and $\Delta_{RN,0}$ respectively. The band gap, both fit (solid lines) and values from measurements (circles), for the model assuming constant β and the self-consistent form which includes an n-dependent band gap is shown in figure 6(a). Renormalized gap estimates were obtained using measured optical gaps and estimates of the electrochemical potential, ζ (shown in figure 6(b)). Here, we can see the effect of the band-nonparabolicity as an increasing band mass as the chemical potential raises. This is based on the assumption of a constant band edge effective mass: $\frac{m_0^*}{m_0} = \frac{E_g}{2p^2}$, which there is reasonable evidence for based on the Seebeck versus n_H Pisarenko plot. At higher carrier concentrations ($>6 \times 10^{19}$ cm^{-3}), the renormalized band gap value becomes quite small, and errors become larger. Therefore, the fact that $E_g(n)$ levels out at about 0.15 eV may not be entirely accurate since the renormalization effect is probably overestimated at these doping levels. Further, PbTe is known to deviate from the Kane model for carrier concentrations greater than this value [16]. As in the constant β case, the empirical $n^{1/3}$ model may be an oversimplification in the case of increasingly narrow gap and/or the simplified Kane model of Ravich may also be an oversimplification which cannot account for these narrowing phenomena.

In the discussion of electronic band structure it is typically a good first approximation to assume the energy bands remain unaltered with doping—the rigid band approximation. Lee, Mahanti *et al* give some examples where this may not be a good assumption in Na doped PbTe [85], although the picture here is complicated by the variability in supercell

calculations [86]. Even experimental measurements of effective mass can show small changes in band structure when using different dopants (I or La) in PbTe which may be related to a shift in band gap [87].With the goal of band engineering in mind it is important to be able to determine how the band structure is altered as the materials are doped or alloyed. While the rigid band approximation works reasonably well for many purposes, this work demonstrates that the differences between true, optical and thermal band gaps can be different of the order 0.1 eV. Most thermoelectric materials are heavily doped semiconductors, where $E_{g,thermal} > k_B T$. In this case, the electronic transport properties (electrical conductivity, Seebeck coefficient) are determined by a single band. In materials that contain multiple bands, the effect of a changing band gap with doping level will be important in developing a self-consistent transport model. The most obvious effect of a narrower band gap is the increased concentration of minority carriers. In the case of most thermoelectric materials, though, the chemical potential (and thermal band gap) is deep enough into the band to where the minority carrier population is still very small compared to majority carriers. The effects become more apparent at high temperatures when $k_B T \sim E_{g,th}$.

While band gap renormalization is a well-known effect that has been studied in many materials, it is generally ignored in thermoelectric materials in favor of the rigid band approximation. This work suggests that in PbTe, both approximations may play a role. While it seems unlikely that the band gap in these materials might become very small (<0.1 eV), it is possible that if the material is sufficiently doped that bipolar effects can be suppressed and a reduced band gap would not be observed by measuring transport properties alone. Ultimately, the apparent discrepancy between the rigid band approximation and band gap renormalization may need to be resolved with either better estimates of the n-dependent chemical potential (using a six band model, rather than the Kane model), or by developing models that more accurately represent renormalization in narrow gap semiconductors. While the constant β single band Kane model does show a much lower chemical potential increase with doping, there is still a significant renormalization leading towards zero gap at very high doping levels, even when the self-consistent solution is considered. This probably is an artifact of the renormalization fit which is best for doping levels less than 6×10^{19} cm^{-3}. While the $n^{1/3}$ scaling law works well in a free electron gas [80], there may be some corrections for narrow gap semiconductors—particularly as the gap becomes small. Even though band gap narrowing is thought to be well understood, the effects in narrow gap semiconductors—as most thermoelectric materials are—are difficult to reconcile with other measurements. Perhaps more experimental and theoretical work should be done to investigate what is different in narrow gap, heavily doped semiconductors from other wider gap materials.

4. Conclusions

While the DRIFTS method of measuring the optical absorption has been thoroughly explored in catalysis research and has shown some promise for quantifying chemical reactions [88, 89], as a technique for precisely determining band gaps in semiconductors diffuse reflectance has only proven semi-quantitative (± 0.1 eV) [90]. In this work, we detect shifts in band gap with doping of smaller than 0.01 eV in PbTe which can be analyzed and understood by methods consistent with current optical literature.

While electronic transport measurements are essential to determine the thermoelectric properties for a materials, optical properties can provide more direct knowledge about the

band structure. Although diffuse reflectance measurements have been used in the thermoelectric literature, it is important to account for the effects of electron population on the absorption edge that alters the observed optical band gap. We have shown a series of iodine doped PbTe samples which show a Burstein–Moss shift in the absorption edge to higher frequencies. Using estimates of the chemical potential from transport measurements, it is possible to estimate that a gap shrinkage of up to 0.15 eV occurs at the highest doping levels appropriate to thermoelectrics. This is observed both by fitting the optical band gap using the Tauc method and by fitting the band gap directly from the spectrally dependent absorption coefficient with a Fermi function. An attempt is made to fit the true gap self-consistently using a single band Kane model which results in a slight reduction in the renormalization. While renormalization has been shown to fit well-behaved empirical models for many semiconductors, PbTe (and possibly other narrow gap materials) exhibits a Burstein–Moss shift and renormalization that are not readily explained with existing theory.

Acknowledgments

The authors acknowledge Gerald Mahan, for his help in discussing renormalization effects. Optical measurements in this work were done in the Molecular Materials Research Center (MMRC) at Caltech's Beckman Institute with support from NASA/Jet Propulsion Laboratory and AFOSR MURI FA9550-10-1-0533. The authors also acknowledge helpful discussions with Yanzhong Pei and Heng Wang.

References

[1] Pei Y Z *et al* 2011 Convergence of electronic bands for high performance bulk thermoelectrics *Nature* **473** 66–9
[2] Pei Y Z *et al* 2011 Stabilizing the optimal carrier concentration for high thermoelectric efficiency *Adv. Mater.* **23** 5674–8
[3] Liu W *et al* 2012 Convergence of conduction bands as a means of enhancing thermoelectric performance of n-type $Mg_2Si_{1-x}Sn_x$ solid solutions *Phys. Rev. Lett.* **108** 166601
[4] Pei Y, Wang H and Snyder G J 2012 Band engineering of thermoelectric materials *Adv. Mater.* **24** 6125–35
[5] LaLonde A D *et al* 2011 Lead telluride alloy thermoelectrics *Mater. Today* **14** 526–32
[6] Biswas K *et al* 2011 Strained endotaxial nanostructures with high thermoelectric figure of merit *Nature Chem.* **3** 160–6
[7] Kanatzidis M G 2010 Nanostructured thermoelectrics: the new paradigm? *Chem. Mater.* **22** 648–59
[8] Crocker A J and Rogers L M 1968 Valence band structure of PbTe *J. Physique* **11–12** C4–129
[9] Veis A N and Ukhanov Y I 1976 Study of absorption-coefficient of p-type PbTe *Sov. Phys. Semicond.—USSR* **10** 780–3
[10] Ravich Y I, Efimova B A and Smirnov I A 1970 Semiconducting lead chalcogenides monographs *Semiconductor Physics* vol 5 ed L S Stil'bans (New York: Plenum) p 377
[11] Singh D J 2010 Doping-dependent thermopower of PbTe from Boltzmann transport calculations *Phys. Rev.* B **81** 195217
[12] Ahmad S *et al* 2006 *Ab initio* studies of the electronic structure of defects in PbTe *Phys. Rev.* B **74** 155205
[13] Hoang K and Mahanti S D 2008 Electronic structure of Ga-, In-Tl-doped PbTe: a supercell study of the impurity bands *Phys. Rev.* B **78** 085111
[14] Hummer K, Gruneis A and Kresse G 2007 Structural and electronic properties of lead chalcogenides from first principles *Phys. Rev.* B **75** 195211

[15] Lusakowski A, Boguslawski P and Radzynski T 2011 Calculated electronic structure of $Pb_{1-x}Mn_xTe$ ($0 \leqslant x < 11\%$): the role of L and Sigma valence band maxima *Phys. Rev.* B **83** 115206
[16] Khoklov D and Ravich Y I 2003 Lead chalcogenides: physics applications *Optoelectronic Properties of Semiconductors and Superlattices* vol 18 ed M O Manasreh (New York: Taylor and Francis) pp 3–34
[17] Nimtz G and Schlicht B 1983 Narrow-gap lead salts *Springer Tracts Mod. Phys.* **98** 1–117
[18] Ekuma C E *et al* 2012 Optical properties of PbTe and PbSe *Phys. Rev.* B **85** 085205
[19] Goldsmid H J 2010 *Thermoelectrics: Basic Principles and New Materials Developments* (*Springer Series in Materials Science*) ed R Hull *et al* (Berlin: Springer) pp 42–4
[20] Goldschmid H J 2010 *Introduction to Thermoelectricity,* (*Springer Series in Materials Science*) ed R Hull *et al* (Berlin: Springer) pp 51–3
[21] Clark M A and Cashman R J 1952 Transmission and spectral response of lead sulfide and lead telluride *Phys. Rev.* **85** 1043–4
[22] Gibson A F 1952 The absorption spectra of single crystals of lead sulphide, selenide and telluride *Proc. Phys. Soc. Lond.* B **65** 378–88
[23] Scanlon W W 1959 Recent advances in the optical and electronic properties of PbS, PbSe, PbTe and their alloys *J. Phys. Chem. Solids* **8** 423–8
[24] Stern F 1961 Optical properties of lead-salt and III–V semiconductors *J. Appl. Phys.* **32** 2166
[25] Prakash V 1967 The optical absorption edge in the lead salts and its variation with temperature and pressure *Technical Report* Defense Technical Information Center
[26] Kim H and Kaviany M 2012 Effect of thermal disorder on high figure of merit in PbTe *Phys. Rev.* B **86** 045213
[27] Nikolić P M 1971 *Some Optical Properties of Lead-Tin-Chalcogenide Alloys* (Belgrade: Publications de la Faculté D'Electrotechnique de l'Université à Belgrade) pp 51–121
[28] Nikolic P M 1966 Solid solutions of CdSe and CdTe in PbTe and their optical properties *Br. J. Appl. Phys.* **17** 341
[29] Nikolic P M 1969 Solid solution of lead–germanium chalcogenide alloys and some of their optical properties *J. Phys. D: Appl. Phys.* **2** 383
[30] Drabkin I A, Zakharyugina G F and Nelson I V 1971 Optical width of the forbidden band of $Pb_{1-x}Mn_xTe$ solid solutions *Sov. Phys. Semicond.—USSR* **5** 277–8
[31] Riedl H R 1962 Free-carrier absorption in p-type PbTe *Phys. Rev.* **127** 162–6
[32] Veis A N *et al* 1976 Investigation of the absorption coefficient of indium-doped PbTe *Sov. Phys. Semicond.—USSR* **10** 62–5
[33] Bocharova T V *et al* 1981 Investigation of the absorption coefficient of thin indium-doped PbTe films *Sov. Phys. Semicond.—USSR* **15** 103–5
[34] Kaidanov V I and Ravich Y I 1985 Deep and resonance states in A(IV)B(VI) semiconductors *Sov. Phys. Usp.* **28** 31–53
[35] Nemov S A and Ravich Y I 1998 Thallium dopant in lead chalcogenides: investigation methods and peculiarities *Phys.—Usp.* **41** 735–59
[36] Yuan S *et al* 1994 Electronic and optical-properties of Pbte/$Pb_{1-x}Eu_xTe$ multiple-quantum-well structures *Phys. Rev.* B **49** 5476–89
[37] Suzuki N and Adachi S 1996 Optical constants of $Pb_{1-x}Sn_xTe$ alloys *J. Appl. Phys.* **79** 2065–9
[38] Suryanarayanan R and Das S K 1990 Growth and optical-properties of $Pb_{1-x}Eu_xTe$ films ($0 < x < 0.55$) *J. Appl. Phys.* **67** 1612–4
[39] Ishida A *et al* 1999 PbCaTe films and PbCaTe/PbTe superlattices prepared by hot-wall epitaxy *Japan. J. Appl. Phys.* **38** 4652–5
[40] Maurice T *et al* 1998 Mid infrared optical investigations of $Pb_{1-x}Eu_xSe$ parallel to BaF_2 thin films grown by MBE *Phys. Status Solidi* b **209** 523–34
[41] Tauber R N, Machonis A A and Cadoff I B 1966 Thermal and optical energy gaps in PbTe *J. Appl. Phys.* **37** 4855–60
[42] Nikolic P M 1965 Optical energy gaps lattice parameters and solubility limits of solid solutions of SnSe and GeSe in PbTe and GeSe in SnTe *Br. J. Appl. Phys.* **16** 1075–9

[43] Cardona M and Greenaway D L 1964 Optical properties + band structure of group 4–6 + group 5 materials *Phys. Rev.* **133** 1685–97
[44] Wang J *et al* 2008 Structural, electrical and optical properties of thermally evaporated nanocrystalline PbTe films *J. Appl. Phys.* **104** 053707
[45] Aspnes D E and Cardona M 1968 Electro-optic measurements of PbS PbSe and PbTe *Phys. Rev.* **173** 714–28
[46] Kaiser W and Fan H Y 1955 Infrared absorption of indium antimonide *Phys. Rev.* **98** 966–8
[47] Spitzer W G and Fan H Y 1957 Determination of optical constants and carrier effective mass of semiconductors *Phys. Rev.* **106** 882–90
[48] Palik E D, Mitchell D L and Zemel J N 1964 Magneto-optical studies of band structure of PbS *Phys. Rev.* **135** 763–78
[49] Drabkin I A, Eliseeva Y Y and Nelson I V 1975 Fundamental absorption edge of heavily doped n-type PbTe *Sov. Phys. Semicond.—USSR* **8** 900
[50] Piccoli N, Besson J M and Balkanski M 1974 Optical constants and band gap of PbTe from thin film studies between 25 and 300 K *J. Phys. Chem. Solids* **35** 971–7
[51] Schmid P E 1981 Optical-absorption in heavily doped silicon *Phys. Rev.* B **23** 5531–6
[52] Bugajski M and Lewandowski W 1985 Concentration-dependent absorption and photoluminescence of N-type InP *J. Appl. Phys.* **57** 521–30
[53] Vanoverstraeten R J and Mertens R P 1987 Heavy doping effects in silicon *Solid-State Electron.* **30** 1077–87
[54] Kanatzidis M G *et al* 2009 Improvement in the thermoelectric figure of merit by La/Ag cosubstitution in PbTe *Chem. Mater.* **21** 1361–7
[55] Li Y P *et al* 2012 High thermoelectric performance of solid solutions $CuGa_{1-x}In_xTe_2$ ($x = 0$–1.0) *Appl. Phys. Lett.* **100** 231903
[56] LaLonde A D, Ikeda T and Snyder G J 2011 Rapid consolidation of powdered materials by induction hot pressing *Rev. Sci. Instrum.* **82** 2090–6
[57] LaLonde A D, Pei Y Z and Snyder G J 2011 Reevaluation of $PbTe_{(1-x)}I_{(x)}$ as high performance n-type thermoelectric material *Energy Environ. Sci.* **4** 2090–6
[58] Wang H *et al* 2012 Weak electron–phonon coupling contributing to high thermoelectric performance in n-type PbSe *Proc. Natl Acad. Sci. USA* **109** 9705–9
[59] Wendlandt W and Hecht H 1966 Reflectance spectroscopy *Chemical Analysis* ed P J Elving and I M Kolthoff (New York: Interscience) pp 63–7
[60] Seeger K 1997 *Semiconductor Physics: An Introduction* 6th edn (Heidelberg: Springer) pp 353–6
[61] Lanir M, Lockwood A H and Levinstein H 1978 Absorption-edge shift in lead-tin telluride *Solid State Commun.* **27** 313–6
[62] Herrmann K H, Melzer V and Muller U 1993 Interband and intraband contributions to refractive-index and dispersion in narrow-gap semiconductors *Infrared Phys.* **34** 117–36
[63] Husain M *et al* 2007 Optical, structural and electrical investigations on $PbTe_{1-x}S_x$ alloys *J. Mater. Sci.* **42** 363–7
[64] Wei S H and Zunger A 1997 Electronic and structural anomalies in lead chalcogenides *Phys. Rev.* B **55** 13605–10
[65] Baleva M, Georgiev T and Lashkarev G 1990 On the temperature-dependence of the energy-gap in PbSe and PbTe *J. Phys.: Condens. Matter* **2** 2935–40
[66] Delaire O *et al* 2011 Giant anharmonic phonon scattering in PbTe *Nature Mater.* **10** 614–9
[67] Dash W C and Newman R 1955 Intrinsic optical absorption in single-crystal germanium and silicon at 77 K and 300 K *Phys. Rev.* **99** 1151–5
[68] Veis A N and Ukhanov Y I 1976 Study of absorption-coefficient of p-type PbTe *Sov. Phys. Semicond.—USSR* **10** 780–3
[69] Yu P Y and Cardona M 1996 *Fundamentals of Semiconductors* (Berlin: Springer)
[70] Basu P K 1997 *Theory of Optical Processes in Semiconductors* (*Series on Semiconductor Science and Technology*) ed H Kamimura, R J Nicholas and R H Williams (Oxford: Oxford University Press) p 447

[71] Charache G W *et al* 1999 Moss–Burstein and plasma reflection characteristics of heavily doped n-type $In_xGa_{1-x}As$ and InP_yAs_{1-y} *J. Appl. Phys.* **86** 452–8
[72] Klinghshirn C F 1995 *Semiconductor Optics* (Berlin: Springer)
[73] Casey H C and Stern F 1976 Concentration-dependent absorption and spontaneous emission of heavily doped GaAs *J. Appl. Phys.* **47** 631–43
[74] Berggren K F and Sernelius B E 1981 Band-gap narrowing in heavily doped many-valley semiconductors *Phys. Rev.* B **24** 1971–86
[75] Huang H C, Yee S and Soma M 1990 The carrier effects on the change of refractive-index for n-type GaAs at $\lambda = 1.06$, 1.3 and 1.55μm *J. Appl. Phys.* **67** 1497–503
[76] Luo H T *et al* 2002 Study of band gap narrowing effect in n-GaAs for the application of far-infrared detection *Physica* B **324** 379–86
[77] Munoz M *et al* 2001 Burstein–Moss shift of n-doped $In_{0.53}Ga_{0.47}As$/InP *Phys. Rev.* B **63** 233302
[78] Kudman I and Seidel T 1962 Absorption edge in degenerate p-type GaAs *J. Appl. Phys.* **33** 771–3
[79] Aw S E, Tan H S and Ong C K 1991 Optical-absorption measurements of band-gap shrinkage in moderately and heavily doped silicon *J. Phys.: Condens. Matter* **3** 8213–23
[80] Mahan G D 1980 Energy-gap in Si and Ge- impurity dependence *J. Appl. Phys.* **51** 2634–46
[81] Pankove J I and Aigrain P 1962 Optical absorption of arsenic-doped degenerate germanium *Phys. Rev.* **126** 956–62
[82] Lu J G *et al* 2007 Carrier concentration dependence of band gap shift in n-type ZnO:Al films *J. Appl. Phys.* **101** 083705
[83] Mahan G D 2010 *Condensed Matter in a Nutshell* (Princeton, NJ: Princeton University Press)
[84] Kalt H and Rinker M 1992 Band-gap renormalization in semiconductors with multiple inequivalent valleys *Phys. Rev.* B **45** 1139–54
[85] Lee M S and Mahanti S D 2012 Validity of the rigid band approximation in the study of the thermopower of narrow band gap semiconductors *Phys. Rev.* B **85** 165149
[86] Takagiwa Y *et al* 2012 Dopants effect on the band structure of PbTe thermoelectric material *Appl. Phys. Lett.* **101** 092102
[87] Pei Y *et al* 2012 Low effective mass leading to high thermoelectric performance *Energy Environ. Sci.* **5** 7963–9
[88] White D R and White R L 2008 Isoconversion effective activation energy profiles by variable temperature diffuse reflection infrared spectroscopy *Appl. Spectrosc.* **62** 116–20
[89] White R L 2012 Variable temperature infrared study of copper sulfate pentahydrate dehydration *Thermochim. Acta* **528** 58–62
[90] Boldish S I and White W B 1998 Optical band gaps of selected ternary sulfide minerals *Am. Mineral.* **83** 865–71